An Artificial Neural Network Based Target Angle Estimation Technique for FMCW MIMO Radars

Kudret Akçapınar[1, *], Naime Özben Önhon[2], and Özgür Gürbüz[1]

Abstract—In this paper, an artificial neural network (ANN) based approach is proposed for the estimation of the target angle using Multiple Input Multiple Output (MIMO) radars operating in Frequency Modulated Continuous Wave (FMCW). The proposed technique operates in two stages, with the first stage being the formation of the range profile at each MIMO element via Discrete Fourier Transform (DFT) and the second stage being the estimation of the target azimuth angle via an artificial neural network. The range profile formed in the first stage is fed to the second stage as a single snapshot angle measurement. The performance of the proposed technique is apprised with other existing methods under different Signal-to-Noise Ratio (SNR) conditions and measurement model uncertainties. The simulations performed show that the learning capability of the model strongly hinges on SNR conditions, and the learning process is ameliorated as SNR in training data increases as anticipated. Under low SNR conditions, the proposed technique performs better than other techniques in terms of Mean Square Error (MSE). We have also shown that our solution remains unaffected by the model uncertainties as it fully relies on the calibration data, while the performance of the model-based angle estimation techniques dramatically degrades as the uncertainty in the underlying model grows.

1. INTRODUCTION

Radars have been used in a broad spectrum of sensing applications. These applications may vary from drone detection [1] or runway surveillance to detect the presence of any foreign object debris on a runway [2] to precise surface imaging in industrial areas [3]. Amongst the other radar types, specifically, MIMO radars have recently gained significant momentum due to the angular resolution improvement over the conventional phased array radars. Additionally, MIMO radars provide waveform diversity enabling significant superiority over its phased-array counterpart in terms of improved parameter identifiability [4].

With an array of antennas, it is possible to find the direction of incident signals without the necessity of highly directional antennas being mechanically steered. The direction of arrival (DoA) of signals is achieved by digital beamforming algorithms in antenna arrays. This problem has been extensively studied in the literature of array signal processing. Consequently, several DoA algorithms applicable to the MIMO radar context already exist. The classical approaches are conventional beamformer (Barlett) as described in [5], Estimation of Signal Parameters via Rotational Invariance Technique (ESPRIT) in [6] and Multiple Signal Classification (MUSIC) in [7]. A detailed study on the comparison of these algorithms can be found in [8]. Another class of techniques developed for the solution of DoA problems consists of sparsity-based approaches, which have also been studied in the MIMO radar context as in [9, 10]. The compressive-sensing based approaches provide quite good results, particularly for the cases in which the azimuth spectrum of the arrival signals is known to be sparse as *a priori*. On the

[1] Faculty of Engineering and Natural Sciences, Sabancı University, Tuzla, İstanbul 34956, Türkiye. [2] Faculty of Engineering, Turkish-German University, Beykoz, İstanbul, Türkiye.

other hand, the recent advances in the machine learning frameworks have motivated researchers to seek machine learning-based solutions for the various radar estimation problems as an alternative to the model-based methods. Moreover, machine learning-based solutions are partially or fully data-driven meaning that they do not count on any prior assumption on the underlying measurement model and consequently are expected to be less affected by the possible array imperfections than their model-based counterparts [11]. Therefore, learning-based parameter estimation in the MIMO radar context has drawn significant attention. For instance, recently a deep-learning framework has been used in [12] where supervised deep neural networks are used to map the received signals to their DoAs in the MIMO communication system context. Similarly, in [13], a fully connected deep learning model is adept to find the number of signal sources in the sensing environment and their respective directions. [14] uses an ensemble of convolution neural networks to estimate the 2D DoA using a circular array antenna. In [15], the authors propose a deep learning-based super-resolution DoA estimator using single snapshot MIMO radar data.

In principle, one can design perfect arrays to perform all kinds of array processing algorithms; however, when it comes to practice, the performance of array processing algorithms significantly suffer from practical issues. For example, external environmental factors may cause the antenna positions to deviate from their intended positions, giving rise to the array model uncertainties. The uncertainty in the underlying model leads to performance deterioration of the array signal processing algorithms. That being the case, inaccuracies in the model ought to be removed before a MIMO radar is deployed to benefit from its angular resolution advantages to the utmost.

In this paper, we adopt a data-driven approach to the problem of angle estimation of the targets using MIMO radars. Our motivation for such an approach is to prevent angular estimation performance from being impacted by any inaccuracies in the array shapes. Therefore, in our approach, instead of relying on a measurement model which is highly dependent on the array geometry and calibration of the RF components, motivated by the works in [13–15] we aim to learn the measurement model directly from the training/calibration data through an artificial neural network. The main contributions of this paper can be listed as follows: 1) Explicit range expressions for the FMCW operation are derived, 2) an artificial neural network-based learning technique for the estimation of target angle using a single snapshot angle measurement is proposed and implemented, 3) performance of the proposed approach under different SNR conditions and model uncertainty in comparison with the existing methods through the extensive end-to-end FMCW MIMO radar simulation performed in the physical layer.

The rest of this manuscript is organized as follows. Our system and signal model is explained in Section 2 along with the derivations of the explicit range expressions for the FMCW operation. Our proposed technique is discussed in detail in Section 3, covering the generation of training data from the radar simulations, details of the neural network used, and the training of the model. Our numerical results are provided in Section 4, and conclusions are given in Section 5.

2. SYSTEM AND SIGNAL MODEL

In this paper, we consider a MIMO radar with co-located uniform linear array (ULA) both at the transmitter and receiver sides is considered. A simplified system model is demonstrated in Figure 1, where Figure 1(a) shows a single transmitter and receiver pair and their respective simplified RF backend circuitry, and Figure 1(b) provides an integral system overview for the MIMO architecture. In this MIMO radar model, transmitting array is equipped with N_t antennas, while receive array is equipped with N_r antennas. The spacing between receiving antennas is d and between transmitting antennas is $N_r \cdot d$, respectively. This special placement of transmitting and receiving antennas forms a virtual array with $N_t \cdot N_r$ antennas. A MIMO radar, therefore, provides a multiplicative gain in the number of virtual array elements hence in turn angular resolution. In principle, one can achieve the same angular resolution with N_t transmitting and N_r receiving antennas as a phased array with $M = N_t \cdot N_r$ since the former and the latter systems are equivalent in terms of angular resolution. We demonstrate the formation of a virtual array with two ULAs and provide the array patterns for an example scenario in Figures 2(a) and 2(b), respectively.

We constrain our study to a target angle estimation problem using an FMCW MIMO radar in a clutter-free environment. In this problem, our aim is to first detect the presence of a target in the
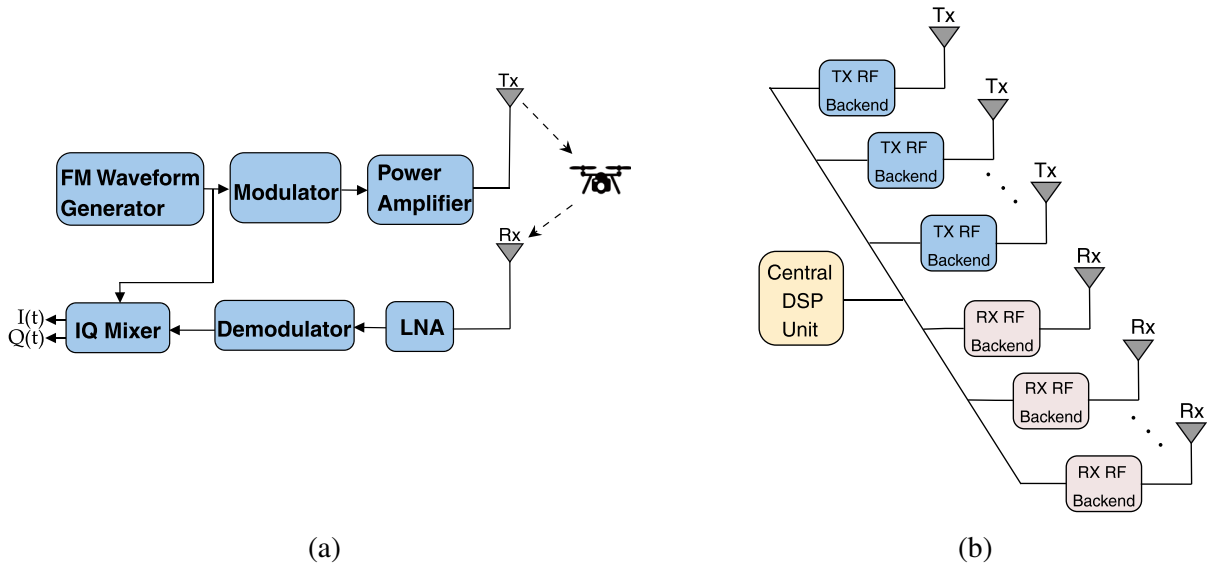
Figure 1. Simplified model of a MIMO radar system. (a) RF backend for a single TX-RX pair. (b) MIMO radar architecture.
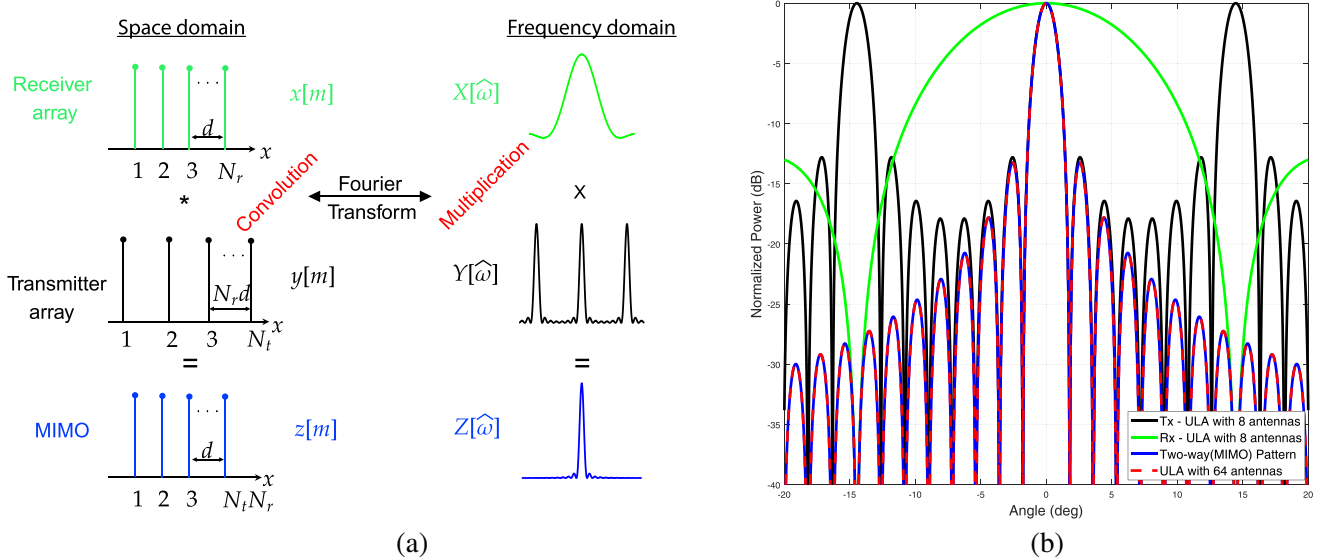

Figure 2. Demonstration of how virtual array/aperture of MIMO radars is created. (a) Demonstration of the equivalence between the array factor of $N_t \times N_R$ MIMO radar and $1 \times N_t N_r$ SIMO radar. (b) Array pattern of an 8×8 MIMO radar array at $24\,\text{GHz}$, $d = 0.5\lambda$.

radar coverage and secondly find the respective range and azimuth information of these targets. The range information is extracted from the principle of FMCW operation while the azimuth angle of the target is determined by a pre-trained artificial neural network. In a typical FMCW radar operation with a single TX and RX antenna first, a chirp signal is generated, up-converted to the radio frequency (RF) band, then amplified and transmitted through the transmitter antenna. On the receiving side, the reflected signal picked up by the receiver antenna is first passed through a low-noise amplifier, then down-converted to the baseband, and finally mixed with the transmitted signal to create in-phase $I(t)$ and quadrature $Q(t)$ components of the received signal, as shown in Figure 1(a). An FMCW radar
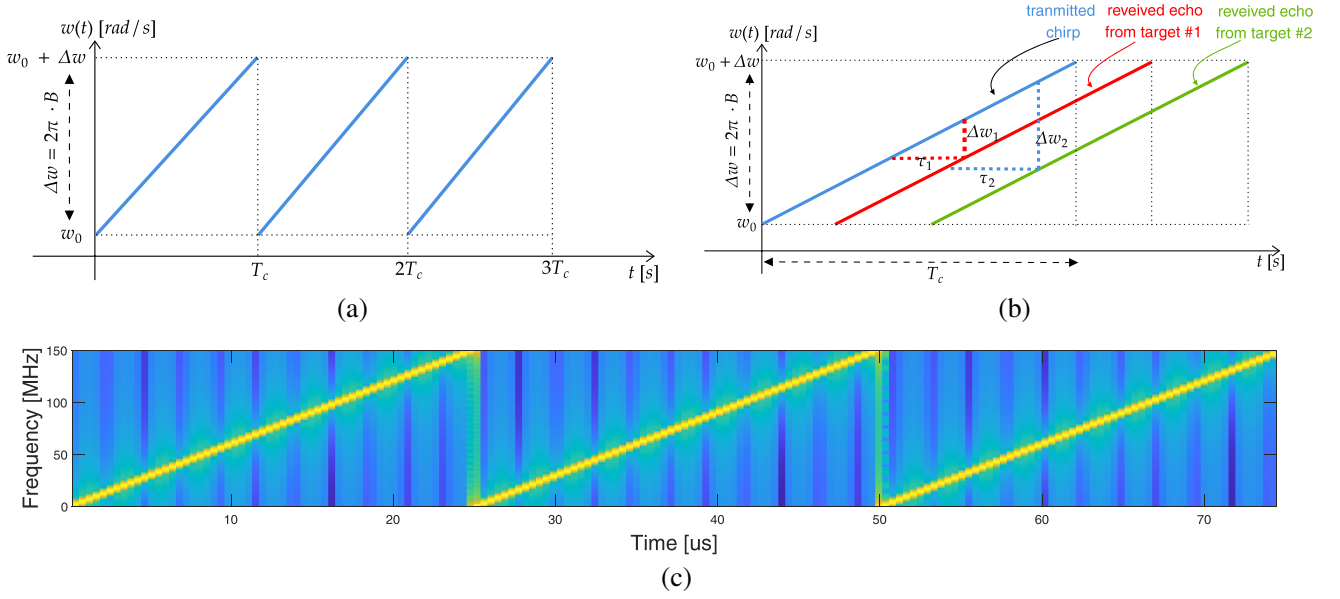
Figure 3. Linear up-chirp FMCW signal considered in our simulations. (a) Transmission cycle with linear up-chirps. (b) Echo signals due to two targets at different ranges. (c) Spectrogram of three cycles of the transmit signal used in the simulations.

transmits a sequence of chirps with the following mathematical expression,

$$s(t) = \sum_{n=0}^{N} s_p(t - nT_c), \text{ with } s_p(t) = (U(t) - U(t - T_c)) \cos(\Phi(t)), \quad t \in [0, T_c]$$

where $U(t)$ denotes the unit step function, T_c the chirp period, and N the number of chirp pulses to be transmitted. The instantaneous angular frequency is given by $\omega(t) = \frac{d\Phi(t)}{dt}$. If the $\omega(t)$ is selected as linearly increasing in time with a slope of m, i.e., $\omega(t) = \omega_0 + mt$ then by integrating $w(t)$ with respect to t, then we get $\Phi(t) = \omega_0 t + \frac{1}{2}mt^2$ where ω_0 is the initial angular frequency, and m is the slope of the chirp or chirp rate defined as $m = \frac{\Delta\omega}{T_c}$ with $\Delta\omega$ denoting the total angular frequency swept. This can also be expressed as the total bandwidth of the chirp signal in Hertz, $B = \Delta\omega/2\pi$. The instantaneous frequency of the chirp increases for T_c seconds and then returns to its initial value, ω_0 after sweeping a band of $\Delta\omega$. This continuous cycle is shown in Figure 3(a). Let us consider K arbitrary targets, each of which has a radar cross-section (RCS) of σ_i and radial distance to the radar of R_i, $i \in \{1, 2, \ldots, K\}$. The echo signal reflected from the ith target comes back to the radar after a two-way propagation delay of $\tau_i = \frac{2R_i}{c}$ with c denoting the speed of light. In Figure 3(b), the reflected signals from two distinctly located targets are shown. These are time-delayed versions of the transmitted chirp signal. A difference in the frequencies of the transmitted and received signals is observed, proportional to the amount of delay. Since the slope of the chirps is a known quantity, one can determine the time delay based on the frequency shift, from which the distance of the reflector object can be estimated. Considering a single chirp, the received signal at the radar is therefore the superposition of the amplitude-scaled and time-delayed versions of the transmitted signal as follows:

$$r(t) = \sum_{i=1}^{K} G_i \sigma_i \cos\left(\omega_0(t - \tau_i) + \frac{1}{2}m(t - \tau_i)^2 + \theta_i\right) \tag{1}$$

Here G_i entirely captures propagation-related two-way channel effects between the radar and the ith reflector object. The received signal given in expression (1) is next mixed with $\cos(\omega_0 t + \frac{1}{2}mt^2)$ and $\sin(\omega_0 t + \frac{1}{2}mt^2)$ to form in-phase and quadrature components, respectively. Filtering out high-frequency

terms, the received signal is obtained as in-phase and quadrature components as follows:

$$I(t) = \frac{1}{2} \sum_{i=1}^{K} G_i \sigma_i \cos \left(m\tau_i t + \omega_0 \tau_i - \frac{1}{2} m\tau_i^2 \right) \text{ and } Q(t) = \frac{1}{2} \sum_{i=1}^{K} G_i \sigma_i \sin \left(m\tau_i t + \omega_0 \tau_i \frac{1}{2} m\tau_i^2 \right)$$

Using Euler's identity, the complex baseband received signal can then be expressed as

$$r(t) = I(t) + jQ(t) = \frac{1}{2} \sum_{i=1}^{K} G_i \sigma_i \exp \left\{ j \left(m\tau_i t + \omega_0 \tau_i \right) \right\} \tag{2}$$

where we have ignored $\frac{1}{2} m\tau_i^2$ since $4mR_i^2 \ll c^2$. Note that the complex equivalent baseband expression for received signal in (2) states that the received signal at a single antenna is the sum of complex exponential signals whose magnitude, frequency, and phase angle are given by

$$A_i = \frac{G_i \sigma_i}{2}, \quad w_i = m\tau_i = \frac{2 \cdot R_i \cdot \Delta w}{c \cdot T_c} = \frac{4\pi \cdot R_i \cdot B}{c \cdot T_c}, \quad \theta_i = \omega_0 \tau_i = \frac{2\omega_0 R_i}{c} \tag{3}$$

Writing expression in (2) with the newly defined parameters in (3), we have the final form of the complex baseband equivalent of the received signal, which is often called *beat* signal:

$$r(t) = \sum_{i=1}^{K} A_i \exp \left\{ j \left(\omega_i t + \theta_i \right) \right\} \tag{4}$$

Note that the beat signal given in (4) is in the form of the sum of complex exponential signals, from which the radar range profile can be extracted through Fourier transform. We derive the expressions for range profile data by applying Fourier transform of this signal in the next section.

3. LEARNING-BASED ESTIMATION OF TARGET ANGLE

The incoming angle of an incident radio wave can be determined by using a receiver array. The signal described in expression (4) reaches each receiver antenna with time-delay, causing phase differences depending on the linear spacing between MIMO elements and operating frequency. From the phase differences observed at the receivers, it is possible to estimate the direction of arrival of an incoming signal using the angle of arrival estimation methods, the majority of which rely on the measurement model. However, the disadvantage of all the model-based approaches is that any uncertainty in the underlying measurement model leads to estimation inaccuracies. For instance, coarsely displaced antenna elements or insufficiently calibrated RF components lead to model inaccuracies when they are considered calibrated, and computations are performed accordingly. To address the issues concerning model inaccuracies, we propose a data-driven learning-based approach where it is aimed to learn the model completely from the collected data contrary to the conventional model-based approaches. Instead of relying upon a sensing model, we rather try to learn the model from the collected training/calibration data through an artificial neural network. We explain the signal processing steps and how we use neural networks for the estimation of target angles with a MIMO radar in the subsequent sections.

We start our development with the received signal model described in expression (4), which suggests that the frequency content of the received signal contains the range information of the targets. In order to perform digital signal processing, the received signal is sampled at a sampling rate of $F_s = \frac{1}{T_s}$, with T_s being the sampling period. During each chirp cycle, a total of $N_s = T_c \cdot T_s$ samples are collected. The sampled beat signal can be expressed in discrete time by replacing t with nT_s

$$r[n] = r(t) \Big|_{t=nT_s} = \sum_{i=1}^{K} A_i \exp \left\{ j \left(\hat{\omega}_i n + \theta_i \right) \right\}, \quad 0 \leq n < N_s \tag{5}$$

where $\hat{\omega} = \omega T_s$ denotes the normalized angular frequency. The Fourier transform of this signal is

$$R(\hat{\omega}) = \mathcal{F}\{r[n]\} = \sum_{n=0}^{N_s-1} r[n] e^{-j\hat{\omega}n} = \sum_{n=0}^{N_s-1} \sum_{i=1}^{K} A_i \exp \left\{ j \left(\hat{\omega}_i n + \theta_i \right) \right\} e^{-j\hat{\omega}n}$$

$$= \sum_{i=1}^{K} A_i e^{j\theta_i} \sum_{n=0}^{N_s-1} e^{j\hat{\omega}_i n} e^{-j\hat{w}n} = \sum_{i=1}^{K} A_i e^{j\theta_i} \underbrace{\sum_{n=0}^{N_s-1} e^{-jn(\hat{w}-\hat{\omega}_i)}}_{P_{N_s}(\hat{\omega}-\hat{\omega}_i)} = \sum_{i=1}^{K} A_i e^{\theta_i} P_{N_s}(\hat{\omega}-\hat{\omega}_i) \tag{6}$$

where $P_{N_s}(\hat{\omega}-\hat{\omega}_i)$ is the sinc pulse whose center is shifted by $\hat{\omega}_i$ in $\hat{\omega}$ as shown in [16]

$$P_{N_s}(\hat{\omega}) = \sum_{i=0}^{N_s-1} e^{-jn\hat{\omega}} = \frac{\sin(\hat{\omega}N_s/2)}{\sin(\hat{\omega}/2)} \exp\{-j\hat{\omega}(N_s-1)/2\} \tag{7}$$

Note that $P_{N_s}(\hat{\omega})$ is the Fourier transform of the N_s-point rectangle window. Similarly, by sampling normalized angular frequency such that $\hat{\omega} = \frac{2\pi k}{N_s}$, Fourier transform expressed in continuous frequency in expression (6) can be converted to discrete frequency as follows

$$R[k] = R(\hat{\omega})\Big|_{\hat{\omega}=\frac{2\pi k}{N_s}} = \sum_{i=1}^{K} A_i e^{\theta_i} P_{N_s}\left(\frac{2\pi k}{N_s} - \hat{\omega}_i\right), \quad 0 \le k < N_s \tag{8}$$

Here k denotes the discrete frequency index and can be related to the true radial distance values, denoted by $d[k]$ through the following relation

$$d[k] = \frac{c \cdot w \cdot T_c}{2 \cdot \Delta w} = \frac{c \cdot f_k \cdot T_c}{2 \cdot B} = \frac{c \cdot T_c \cdot F_s}{2 \cdot B \cdot N_s} k = \frac{c}{2B} k, \quad 0 \le k < N_s \tag{9}$$

It is worthwhile to note that the expression given in discrete Fourier domain by (8) is the sum of sinc pulses shifted in frequency with an amount from which any reflector object's radial distance to the radar can be determined. This expression is important in the sense that it contains range profile, which is fed to our DoA neural network as the input. That is, distance and response vectors $\{d[k], R[k]\}$ together provide complete information regarding the range profile of the radar scene when $|R[k]|$ is plotted against $d[k]$. At each MIMO element, Fourier transform is performed on the received signal in (4) using Fast Fourier Transform (FFT) to obtain the range profile given by (8), and the FFT results are stored in a data matrix, $\mathbf{D}(r,m) \in \mathcal{C}^{R \times M}$ where $r = \{1, 2, \ldots, R\}$ is the range index, and $m = \{1, 2, \ldots, M\}$ is the index for the each MIMO Tx-Rx pair. Columns of the data matrix are the range profile seen by the corresponding antenna pair, while the rows correspond to the single snapshot angle measurements. On the data matrix, a peak detection algorithm is run along the range axis, and if a target is detected, then the complex snapshot measurements at each detection range cell are fed into a neural network to estimate the angle of the target. These steps are depicted in Figure 4, with details provided in Algorithm 1.

Algorithm 1: Steps of the proposed DoA estimation technique

---

1 Initialize the radar data matrix, $\mathbf{D} \leftarrow \mathbf{0}(R, M)$.
2 For each Tx-Rx pair, take the FFT of the received signal and store it in the columns of $\mathbf{D}$.
3 Perform a target detection algorithm on $\mathbf{D}$ along the range dimension.
4 Take the angle measurements at the detected range cells and store it in $\mathbf{v} \in \mathcal{C}^{1xM}$.
5 Normalize $\mathbf{v}$ with respect to the measurement at the 1$^{\text{st}}$ MIMO element, $\overline{\mathbf{v}} = \frac{\mathbf{v}}{|\mathbf{v}(1)|}$.
6 Concatenate real and imaginary parts of $\mathbf{v}$, $\mathbf{w} = \text{conc}(\text{Re}\{\overline{\mathbf{v}}\}, \text{Im}\{\overline{\mathbf{v}}\})$.
7 Feed $\mathbf{w}$ to pre-trained ANN to estimate target angle $\hat{\theta} = \sigma(\mathbf{w})$.
8 Return to step 4 and repeat the procedure for each detection.

Depending on the azimuth angle of a target, the snapshot angle measurements at the respective range cell of the target show different patterns. An artificial neural network is believed to learn the relation between these snapshot measurement patterns and the respective target angle. To better illustrate these patterns, we demonstrate 4 different snapshot angle measurements of a single target at 4 different azimuth angles from a 6×10 MIMO radar in Figure 5. Here, the number next to each measurement mark represents the corresponding MIMO index. It should also be noted that the snapshot

Figure 4. Data processing steps of the proposed method: 1) Range extraction through FFT along the fast-time axis. 2) Target detection. 3) DoA estimation with the trained neural network.
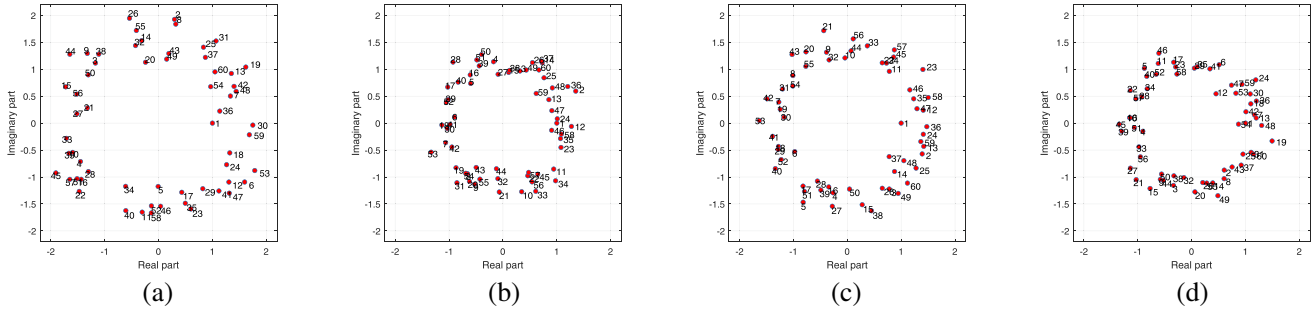

Figure 5. Normalized single snapshot measurements of a point target located at different azimuth angles in complex plane. Each marker indicates the phase angle of the received at the MIMO elements. (a) Single target placed at azimuth angle $-20°$. (b) Single target placed at azimuth angle $-10°$. (c) Single target placed at azimuth angle $10°$. (d) Single target placed at azimuth angle $20°$.

angle measurements are normalized with respect to 1st MIMO element to make the measurements range-independent.

In terms of computational complexity, steps 2 and 7 are the dominant processing steps. Step 2 is where the radar matrix is converted into range profiles at each MIMO element and is the common step for all the DoA methods investigated. This step has an asymptotic complexity of $\mathcal{O}(M \times R \times \log R)$. In step 7 complex MIMO measurements at the detected range cell are passed through ANN, whose complexity depends on the selected neural network and the number of neurons at each layer. We provide a practical computation time analysis for the neural network used in our simulations in Section 4.2.

In order to learn the relation between snapshot angle measurements and the target azimuth angle, we use a fully connected neural network with a single hidden layer. Assuming that $M = N_t \cdot N_r$ is the virtual MIMO array size, the input layer has $2M$ neurons, where the first M input neurons take the real part of the angle measurements, and the last M neurons take the imaginary part of the measurements. The output layer is a single neuron, which generates the estimated target angle. In the hidden layer, the hyperbolic tangent sigmoid function is used while in the output layer linear activation function is used.

4. NUMERICAL RESULTS

In this section, we explain our MIMO radar simulation environment and how we acquire the MIMO radar data to be used in the training of the neural network. We also compare the performance of our proposed approach with the other existing DoA algorithms over the investigated simulation scenarios.

4.1. Training Data Generation and Network Training

For the generation of the training data, we consider a virtual anechoic chamber environment where the reflector object can be rotated around the MIMO radar, and echo signals are collected at each position for several pulses. In our simulation, we do this by randomly positioning a target around the radar. For each position of the target, a different measurement is obtained, as depicted in Figure 5. All these position-measurement pairs form the training/calibration data.

In order to create a training data set, we performed physical layer-level end-to-end MIMO radar simulations using the Phased Array System Toolbox of Matlab 2021b. In simulations both the radar

Table 1. Radar parameters used in the MIMO radar simulations.

Parameters	Value	Parameters	Value
Frequency	24 GHz	Peak power	200 mW
Number of Tx antennas	6	Tx gain	0 dB
Number of Rx antennas	10	Rx gain	0 dB
Number of Virtual MIMO elements	60	Noise figure	0 dB
Sweep time	25 μs	Sampling rate	300 MHz
Sweep bandwidth	150 MHz	Range resolution	1 m
Chirp rate	6×10^{12}	Max. allowed range	750 m

and target objects are kept stationary, i.e., no Doppler effect is allowed. For the simulation of the two-way channel, we assume a free-space model and consider a 6×10 MIMO radar where the transmissions take place in turn, with each transmitter taking the channel in the non-overlapping time slots. Radar-related simulation parameters are summarized in Table 1. We consider a linear FMCW signal for the transmission with a sweep bandwidth of 150 MHz and a chirp period of 25 μs, as shown in Figure 3(c). In the simulations, a single chirp waveform transmitted from each antenna is collected by each receiver simultaneously after reflecting from the target object. Receiver noise is assumed to be complex Additive White Gaussian Noise (AWGN). We run 10^4 Monte Carlo simulations in which a single target is placed 250 m away from the radar, and the azimuth angle is uniformly distributed in $[-20°, 20°]$.

The obtained data set is later randomly divided into three sets: a training set of 7500 samples, a test set of 1500 samples, and a validation set of 1500 samples. In order to test the network performance under different SNR conditions, we also form different data sets considering different target RCS values under fixed receiver noise levels. MSE is chosen as the cost function in the optimization. The network is implemented using Deep Learning Toolbox of Matlab 2021b. For each training data set generated with different target RCS levels, a separate network is trained. The MSE cost function during the training is shown in Figure 6 for the same network trained over data sets generated with different RCS values.
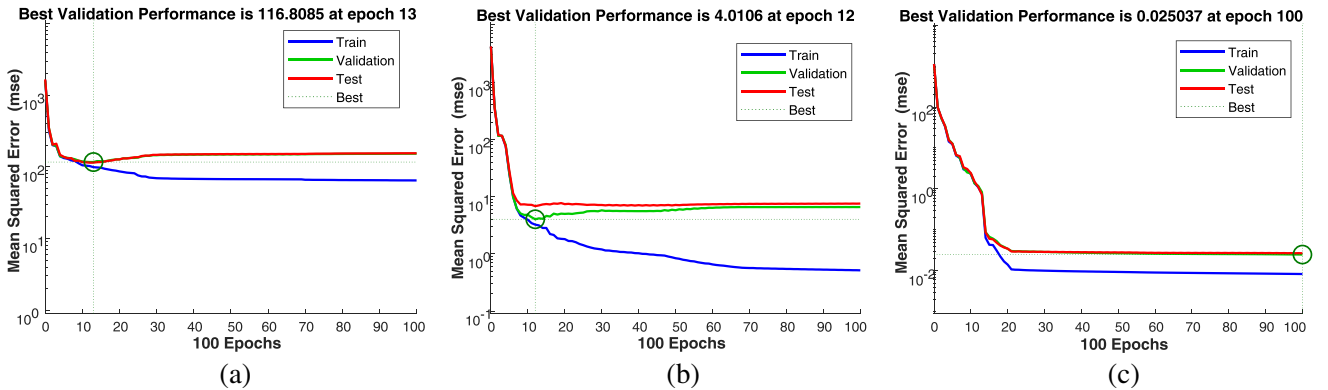

Figure 6. MSE during the training (100 epochs) of the networks under different SNR levels. (a) Network trained for $\sigma = 25$ dbsm. (b) Network trained for $\sigma = 30$ dbsm. (c) Network trained for $\sigma = 40$ dbsm.

4.2. Performance Evaluation

Test performance is assessed in terms of MSE on the test data set which contains 1500 measurement-angle pairs. We first show the validity of our proposed solution under different SNR conditions. The scatter plots in Figure 7 show the correlation between the ground truth and the neural network response. Here the x-coordinate of each data point shows the target azimuth angle (ground truth), and the y-coordinate is the neural network estimation. The correlation coefficient is computed and provided at the
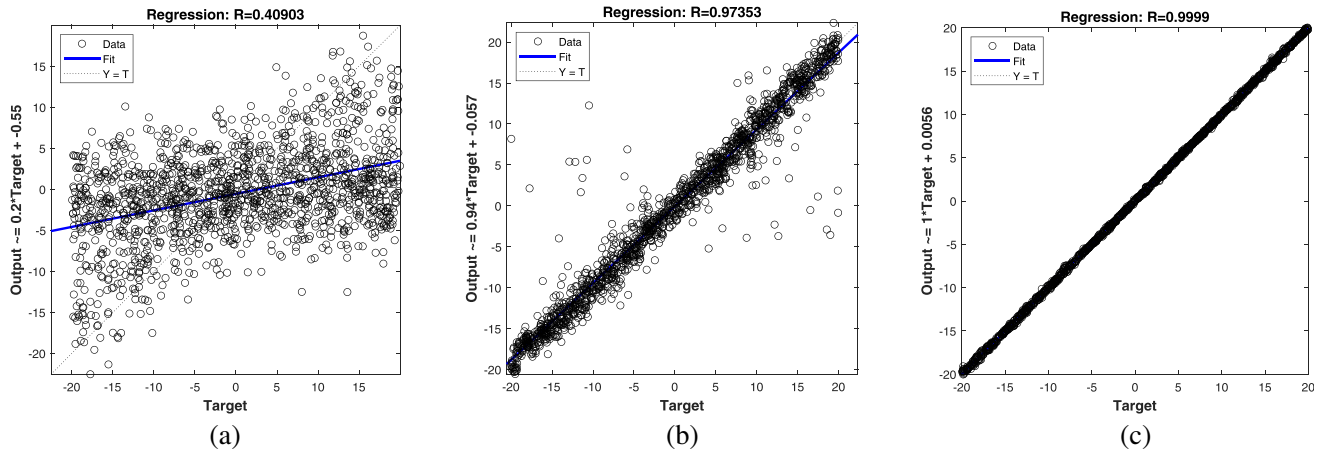
Figure 7. Regression performances of networks trained at different target RCS levels. (a) Network trained for $\sigma = 25$ dbsm. (b) Network trained for $\sigma = 30$ dbsm. (c) Network trained for $\sigma = 40$ dbsm.

Figure 8. Error histograms of the networks trained at different target RCS levels. (a) Network trained for $\sigma = 25$ dbsm. (b) Network trained for $\sigma = 30$ dbsm. (c) Network trained for $\sigma = 40$ dbsm.
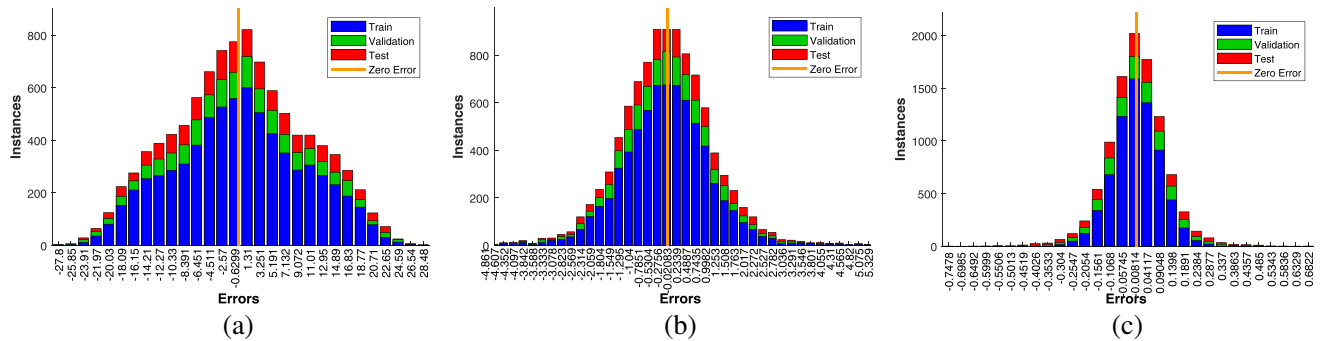
top of each figure. The best line fit is also shown with a blue line in the plots. As SNR in the training data increases, the best line fit gets closer to the line $Y = T$, and the correlation coefficient approaches 1. It clearly shows that the proposed network is able to learn the given task and the estimation accuracy of the model improves with increasing SNR.

Similarly, the error histogram of each neural network is given for train, validation, and test data sets in Figure 8. Here, we define the error as the difference between the model response and the ground truth, i.e., $e = Y - T$. Zero error levels are also indicated with a vertical red line. As seen from the figures, errors exhibit a normal-like distribution around zero. It is also quite clear that as SNR increases in the training data set, the learning performance of the network improves, which leads to a smaller error standard deviation.

Having validated the model and its learning capability by checking the estimation accuracy in incremental SNR conditions, we next compare the MSE performance of the proposed technique with the other existing model-based DoA algorithms for different SNR and model uncertainty levels. The results are shown in Figure 9. The MSE values are the average values, calculated by averaging over 1500 test samples. Each green diamond mark in the plots represents the performance of the neural network trained for that specific scenario. MSE performances of the different methods are evaluated under different SNR conditions in Figure 9(a). Under low SNR conditions, the proposed technique shows superior performance in terms of MSE as compared to the other benchmark methods. In Figure 9(b), we present the effect of the model uncertainty. In order to introduce model uncertainty, we corrupt the phase of measurements at each MIMO element by adding random phases to the measurements and use
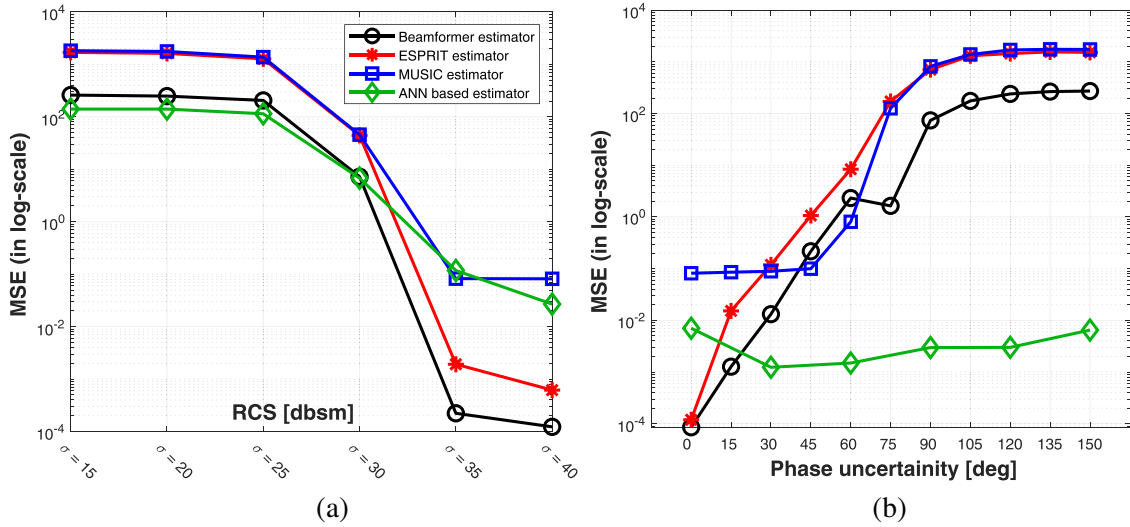
Figure 9. Performance comparison of the proposed technique with other existing DoA methods. (a) MSE vs. target RCS. (b) MSE vs. model uncertainty.

the standard deviation of the phase randomness as a metric to quantify the model uncertainty, as shown in the x-axis of the plot in Figure 9(b). In practice, these model uncertainties could stem from perturbed antenna positions or poorly calibrated RF circuitry. Apparently, performances of all the model-based DoA methods deteriorate as the uncertainty in the underlying model increases. On the other hand, the proposed neural network based solution shows almost no dependency on the uncertainty in the model. This can be explained by the fact that the proposed method truly relies on the training data, which already contains model uncertainties in it. In other words, since the proposed method learns the mapping from the measurements to the azimuth angle of the targets directly from the calibration data, it remains unaffected by the model uncertainties while all the model-based methods strictly depend on how accurately the underlying measurement model is known.

For applications where computation and memory budget is limited, the complexity of the employed algorithms becomes quite critical. Therefore, in addition to MSE performance of the proposed method, we have also evaluated the computational complexity of our DoA method in a practical manner. For this purpose, we take one of the test data sets and ran all the methods on a 3.4 GHz Quad-Core Intel Core i5 processor and measured the time elapsed during the execution of each method. The averaged elapsed times are given in Table 2. The proposed method was shown to consume only 5 ms more CPU time than the other methods. The neural network that we use for the DoA estimation of radar targets consists of total $2420(120 \times 20 + 20)$ weights and 21 biases. Assuming that weight and bias parameters have double precision (8 bytes), our neural network requires approximately 19 KBytes of RAM. The memory consumption of the other DoA methods can be found in [17].

Table 2. The average computation times of DoA methods, calculated with 1500 runs of each method.

Beamformer Estimator	ESPRIT Estimator	MUSIC estimator	ANN based estimator
699.2 ms	700.33 ms	700 ms	705 ms

4.3. Extension to 2D DoA

In many applications, it is also desirable to have a 2D DoA estimation, i.e., both azimuth (θ) and elevation (ϕ) angles of the radar target with respect to the radar. We show how our proposed method can be extended to cover also 2D DoA estimation. It is necessary to distribute the MIMO radar

antennas over a plane instead of along a line for 2D DoA estimation. Therefore, we consider a 'plus' shape antenna array with 4 TX antenna and 4 RX antenna placed on the x and y axes. For the MIMO configuration, RX antennas are separated by $\lambda/2$ while TX antennas are separated by $3\lambda/2$. This way we would achieve a virtual aperture of 16 antennas along both the x and y directions. We use the same algorithm as given in Algorithm 1 with only difference being the neural network structure. For this 2D DoA estimation network, the input layer has 32 neurons for the real part of the measurements and 32 neurons for the imaginary part, making it total of 64 neurons in the input layer. The other difference is the output layer, which has two neurons to account for the azimuth and elevation angles of the target. Over a simulated training data set, we train the 2D DoA network and test its performance over the test data set. Figure 10(a) shows the MSE error during training, while Figure 10(b) shows the estimation error for θ and ϕ. As it is clear from Figure 10, learning is achieved with a significantly small MSE, and error histogram plot shows a normal distribution around zero with very low variance. With this, we verify the applicability of our proposed technique also for the 2D DoA estimation problems.
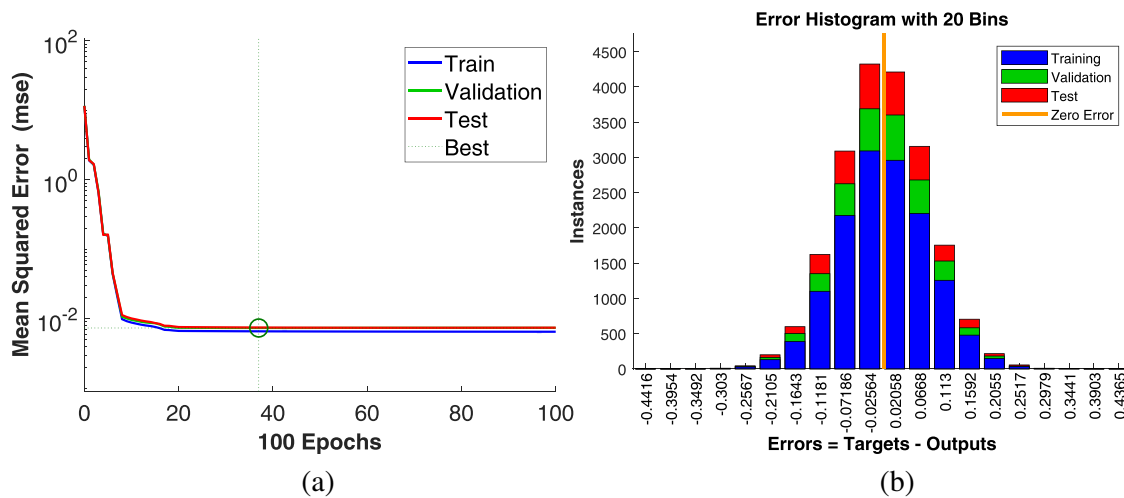

Figure 10. Training and test results of the network for 2D DoA estimation. (a) Training of 2D DoA network. (b) Error histograms.

5. CONCLUSIONS

A neural network-based target 1D angle estimation technique is proposed in this paper to overcome the practical issues in MIMO radars caused by imperfect array shapes or poorly calibrated RF components. The proposed technique proceeds in two stages with range profile formation being the first stage fed to the second stage as the input for the ANN model. Our ANN model is trained on the simulated data generated by the MIMO radar simulations performed in the physical layer under different SNR conditions and model inaccuracies. The numerical results suggest that the proposed technique performs better than the other existing DoA estimation techniques in low SNR scenarios. More importantly, the proposed technique is shown to remain almost unaffected by the model perturbations/inaccuracies caused by the external factors given that network is trained over the data generated with the same simulation configuration as the test set. It was demonstrated that while the performance of all the model-based DoA estimation techniques dramatically deteriorates, the proposed technique is proven to be independent of the underlying model since it learns the relation between the measurements and the target angle directly from the training data. Finally, we also show the applicability of our proposed ANN based DoA method to the 2D DoA estimation with a 2D MIMO radar array.

REFERENCES

1. Wang, S. and R. Herschel, "Fast 3D-CFAR for drone detection with MIMO radars," *2021 18th European Radar Conference (EuRAD)*, 209–212, 2022, doi: 10.23919/EuRAD50154.2022.9784486.

2. Akçapınar, K. and S. Baykut, "CM-CFAR parameter learning based square-law detector for foreign object debris radar," *2018 15th European Radar Conference (EuRAD)*, 421–424, 2018, doi: 10.23919/EuRAD.2018.8546514.

3. Zankl, D., S. Schuster, R. Feger, and A. Stelzer, "What a Blast!: A massive MIMO radar system for monitoring the surface in steel industry blast furnaces," *IEEE Microwave Magazine*, Vol. 18, No. 6, 52–69, Sept.–Oct. 2017, doi: 10.1109/MMM.2017.2711998.

4. Li, J. and P. Stoica, "MIMO radar with colocated antennas," *IEEE Signal Processing Magazine*, Vol. 24, No. 5, 106–114, Sept. 2007, doi: 10.1109/MSP.2007.904812.

5. Hassanien, A., M. G. Amin, Y. D. Zhang, and F. Ahmad, "High-resolution single-snapshot DOA estimation in MIMO radar with colocated antennas," *2015 IEEE Radar Conference (RadarCon)*, 1134–1138, 2015, doi: 10.1109/RADAR.2015.7131164.

6. Roy, R. and T. Kailath, "ESPRIT-estimation of signal parameters via rotational invariance techniques," *IEEE Transactions on Acoustics, Speech, and Signal Processing*, Vol. 37, No. 7, 984–995, Jul. 1989, doi: 10.1109/29.32276.

7. Schmidt, R., "Multiple emitter location and signal parameter estimation," *IEEE Transactions on Antennas and Propagation*, Vol. 34, No. 3, 276–280, Mar. 1986, doi: 10.1109/TAP.1986.1143830.

8. Oumar, O. A., M. F. Siyau, and T. P. Sattar, "Comparison between MUSIC and ESPRIT direction of arrival estimation algorithms for wireless communication systems," *The First International Conference on Future Generation Communication Technologies*, 99–103, 2012, doi: 10.1109/FGCT.2012.6476563.

9. Yu, Y., A. P. Petropulu, and H. V. Poor, "MIMO radar using compressive sampling," *IEEE Journal of Selected Topics in Signal Processing*, Vol. 4, No. 1, 146–163, Feb. 2010, doi: 10.1109/JSTSP.2009.2038973.

10. Ni, Z., B. Huang, and M. Cao, "Angular positions estimation of spatially extended targets for MIMO radar using complex spatiotemporal sparse Bayesian learning," *IEEE Access*, Vol. 7, 94473–94480, 2019, doi: 10.1109/ACCESS.2019.2926442.

11. Liu, Z. M., C. Zhang, and P. S. Yu, "Direction-of-arrival estimation based on deep neural networks with robustness to array imperfections," *IEEE Transactions on Antennas and Propagation*, Vol. 66, No. 12, 7315–7327, Dec. 2018, doi: 10.1109/TAP.2018.2874430.

12. Huang, H., J. Yang, H. Huang, Y. Song, and G. Gui, "Deep learning for super-resolution channel estimation and DOA estimation based massive MIMO system," *IEEE Transactions on Vehicular Technology*, Vol. 67, No. 9, 8549–8560, Sept. 2018, doi: 10.1109/TVT.2018.2851783.

13. Bialer, O., N. Garnett, and T. Tirer, "Performance advantages of deep neural networks for angle of arrival estimation," *ICASSP 2019 — 2019 IEEE International Conference on Acoustics, Speech and Signal Processing (ICASSP)*, 3907–3911, 2019, doi: 10.1109/ICASSP.2019.8682604.

14. Zhu, W., M. Zhang, P. Li, and C. Wu, "Two-dimensional DOA estimation via deep ensemble learning," *IEEE Access*, Vol. 8, 124544–124552, 2020, doi: 10.1109/ACCESS.2020.3005221.

15. Ma, Y., Y. Zeng, and S. Sun, "A deep learning based super resolution DoA estimator with single snapshot MIMO radar data," *IEEE Transactions on Vehicular Technology*, Vol. 71, No. 4, 4142–4155, Apr. 2022, doi: 10.1109/TVT.2022.3151674.

16. Li, X., X. Wang, Q. Yang, and S. Fu, "Signal processing for TDM MIMO FMCW millimeter-wave radar sensors," *IEEE Access*, Vol. 9, 167959–167971, 2021, doi: 10.1109/ACCESS.2021.3137387.

17. Al-Sadoon, M. A. G., N. T. Ali, Y. Dama, A. Zuid, S. M. R. Jones, R. A. Abd-Alhameed, and J. M. Noras, "A new low complexity angle of arrival algorithm for 1D and 2D direction estimation in MIMO smart antenna systems," *Sensors (Basel)*, Vol. 17, No. 11, 2631, Nov. 15, 2017, doi: 10.3390/s17112631.